Superdeformed and Triaxial States in ^{42}Ca

K. Hadyńska-Klęk,[1,2,3,4] P. J. Napiorkowski,[1] M. Zielińska,[5,1] J. Srebrny,[1] A. Maj,[6] F. Azaiez,[7] J. J. Valiente Dobón,[4] M. Kicińska-Habior,[2] F. Nowacki,[8] H. Naïdja,[8,9,10] B. Bounthong,[8] T. R. Rodríguez,[11] G. de Angelis,[4] T. Abraham,[1] G. Anil Kumar,[6] D. Bazzacco,[12,13] M. Bellato,[12] D. Bortolato,[12] P. Bednarczyk,[6] G. Benzoni,[14] L. Berti,[4] B. Birkenbach,[15] B. Bruyneel,[15] S. Brambilla,[14] F. Camera,[14,16] J. Chavas,[5] B. Cederwall,[17] L. Charles,[8] M. Ciemała,[6] P. Cocconi,[4] P. Coleman-Smith,[18] A. Colombo,[12] A. Corsi,[14,16] F. C. L. Crespi,[14,16] D. M. Cullen,[19] A. Czermak,[6] P. Désesquelles,[20,21] D. T. Doherty,[5,22] B. Dulny,[6] J. Eberth,[15] E. Farnea,[12,13] B. Fornal,[6] S. Franchoo,[7] A. Gadea,[23] A. Giaz,[14,16] A. Gottardo,[4] X. Grave,[7] J. Grębosz,[6] A. Görgen,[3] M. Gulmini,[4] T. Habermann,[9] H. Hess,[15] R. Isocrate,[12,13] J. Iwanicki,[1] G. Jaworski,[1] D. S. Judson,[24] A. Jungclaus,[25] N. Karkour,[21] M. Kmiecik,[6] D. Karpiński,[2] M. Kisieliński,[1] N. Kondratyev,[26] A. Korichi,[21] M. Komorowska,[1,2] M. Kowalczyk,[1] W. Korten,[5] M. Krzysiek,[6] G. Lehaut,[27] S. Leoni,[14,16] J. Ljungvall,[21] A. Lopez-Martens,[21] S. Lunardi,[12,13] G. Maron,[4] K. Mazurek,[6] R. Menegazzo,[12,13] D. Mengoni,[12] E. Merchán,[9,28] W. Męczyński,[6] C. Michelagnoli,[12,13] J. Mierzejewski,[1] B. Million,[14] S. Myalski,[6] D. R. Napoli,[4] R. Nicolini,[14] M. Niikura,[7] A. Obertelli,[5] S. F. Özmen,[1] M. Palacz,[1] L. Próchniak,[1] A. Pullia,[14,16] B. Quintana,[29] G. Rampazzo,[4] F. Recchia,[12,13] N. Redon,[27] P. Reiter,[15] D. Rosso,[4] K. Rusek,[1] E. Sahin,[4] M.-D. Salsac,[5] P.-A. Söderström,[30] I. Stefan,[7] O. Stézowski,[27] J. Styczeń,[6] Ch. Theisen,[5] N. Toniolo,[4] C. A. Ur,[12,13] V. Vandone,[14,16] R. Wadsworth,[22] B. Wasilewska,[6] A. Wiens,[15] J. L. Wood,[31] K. Wrzosek-Lipska,[1] and M. Zięblińński[6]

[1]*Heavy Ion Laboratory, University of Warsaw, Pasteura 5A, PL 02-093 Warsaw, Poland*
[2]*Faculty of Physics, University of Warsaw, PL 00-681 Warsaw, Poland*
[3]*Department of Physics, University of Oslo, N-0316 Oslo, Norway*
[4]*INFN Laboratori Nazionali di Legnaro, Viale dell'Università, 2, I-35020 Legnaro, Italy*
[5]*CEA Saclay, IRFU/SPhN, F-91191 Gif-sur-Yvette, France*
[6]*Institute of Nuclear Physics, Polish Academy of Sciences, PL 31-342 Kraków, Poland*
[7]*Institut de Physique Nucléaire d'Orsay, F-91400 Orsay, France*
[8]*Université de Strasbourg, IPHC/CNRS, UMR7178, 23 rue du Loess, F-67037 Strasbourg, France*
[9]*GSI Helmholtzzentrum für Schwerionenforschung GmbH, D-64291 Darmstadt, Germany*
[10]*LPMS, Université Constantine 1, Route Ain-El bey, 25000 Constantine, Algeria*
[11]*Universidad Autónoma de Madrid, Departamento de Física Teórica, E-28049 Cantoblanco, Madrid, Spain*
[12]*INFN Sezione di Padova, I-35131 Padova, Italy*
[13]*Dipartimento di Fisica e Astronomia dell'Università degli Studi di Padova, I-35131 Padova, Italy*
[14]*Dipartimento di Fisica dell'Università degli Studi di Milano, I-20133 Milano, Italy*
[15]*Institut für Kernphysik, Universität zu Köln, Zülpicher Straße 77, D-50937 Köln, Germany*
[16]*INFN Sezione di Milano, I-20133 Milano, Italy*
[17]*Department of Physics, Royal Institute of Technology, SE-10691 Stockholm, Sweden*
[18]*Daresbury Laboratory, Daresbury, Warrington WA4 4AD, United Kingdom*
[19]*Schuster Laboratory, School of Physics and Astronomy, The University of Manchester, Manchester M13 9PL, United Kingdom*
[20]*Université Paris-Sud, F-91400 Orsay, France*
[21]*Centre de Spectrométrie Nucléaire et de Spectrométrie de Masse (CSNSM/IN2P3/CNRS), F-91405 Orsay, France*
[22]*Department of Physics University of York, Heslington, York YO10 5DD, United Kingdom*
[23]*Instituto de Física Corpuscular IFIC, CSIC-University of Valencia, S-46980 Paterna, Valencia, Spain*
[24]*Oliver Lodge Laboratory, The University of Liverpool, Liverpool L69 7ZE, United Kingdom*
[25]*Instituto de Estructura de la Materia, CSIC, Madrid, E-28006 Madrid, Spain*
[26]*Flerov Laboratory of Nuclear Reactions JINR, RU-141980 Dubna, Russia*
[27]*Universite Lyon 1, CNRS, IN2P3, IPN Lyon, F-69622 Villeurbanne, France*
[28]*Technische Universität Darmstadt, D-64289 Darmstadt, Germany*
[29]*Laboratorio de Radiaciones Ionizantes, Departamento de Física Fundamental, Universidad de Salamanca, E-37008 Salamanca,Spain*
[30]*Department of Physics and Astronomy, Uppsala University, SE-75120 Uppsala, Sweden*
[31]*School of Physics, Georgia Institute of Technology, Atlanta, Georgia 30332-0430, USA*

(Received 25 March 2016; published 1 August 2016)

Shape parameters of a weakly deformed ground-state band and highly deformed slightly triaxial sideband in ^{42}Ca were determined from $E2$ matrix elements measured in the first low-energy Coulomb excitation experiment performed with AGATA. The picture of two coexisting structures is well reproduced by new state-of-the-art large-scale shell model and beyond-mean-field calculations. Experimental evidence

for superdeformation of the band built on 0_2^+ has been obtained and the role of triaxiality in the $A \sim 40$ mass region is discussed. Furthermore, the potential of Coulomb excitation as a tool to study superdeformation has been demonstrated for the first time.

DOI: 10.1103/PhysRevLett.117.062501

Highly deformed nuclear shapes, of elongation that may be approximately represented as an ellipsoid with a 2:1 major to minor axes ratio, were first observed in fission isomers in 1962 [1]. This discovery was followed by the observation of superdeformed (SD) bands in the rare-earth region [2]. A particularity of these structures, which are found to occur at high spin, was that their linking to the ground-state band was difficult to establish. The phenomenon of superdeformation became a challenge for both experiment and nuclear structure theory, and soon very similar structures were found in other mass regions, namely, $A \sim 130$ [3,4] and $A \sim 190$ [5]. However, the original criterion of a 2:1 axes ratio does not seem to be universally valid, as the deformation of most of the established SD bands corresponds to axes ratios of between 3:2 and 2:1. Recently, SD bands have been discovered in lighter nuclei, particularly in the $A \sim 40$ mass region, where the nucleons occupy similar proton and neutron orbitals. The deformation parameter β in the sidebands of ^{40}Ca [6], ^{36,38,40}Ar [7–10], and ^{44}Ti [11] nuclei reaches 0.4–0.6, which is similar to what is observed in other mass regions, where superdeformation has been established. However, in contrast to heavier nuclei, strongly deformed bands in $A \sim 40$ isotopes are linked to other, less deformed states by intense γ-ray transitions.

Considering the relatively small number of nucleons, the $A \sim 40$ region constitutes an excellent testing ground to study the origin of highly deformed structures within various theoretical approaches, such as, for example, large-scale shell model (SM) [12,13], beyond-mean-field models (BMF) [14–16], and antisymmetrized molecular dynamics (AMD) [17–22]. In particular, the normal-deformed and SD structures in ^{40}Ca were successfully described in the framework of SM calculations that yielded a spherical ground-state band, a normal-deformed band ($\beta = 0.3$) built on the 0_2^+ state dominated by the $4p$-$4h$ excitation into the pf shell, and a SD band ($\beta = 0.6$) built on the 0_3^+ state with an $8p$-$8h$ configuration [13]. The sideband observed in this nucleus at low excitation energy was interpreted as a partner of the $4p$-$4h$ excited band, resulting from its triaxial shape, which is in agreement with the conclusions of other theoretical works [18,23,24]. The importance of the triaxial degree of freedom in the development of deformation was also suggested for other nuclei in this mass region, e.g., ^{44}Ti [17]. The currently available experimental data, however, are not conclusive, as they are mostly limited to energies of states in γ bands. More solid evidence for triaxiality can be obtained from a measurement of transition probabilities and quadrupole moments of excited states.

A regular sideband built on the 0_2^+ state is known in ^{42}Ca, and some of its spectroscopic properties do not differ significantly from those of the established SD bands in the $A \sim 40$ region. Firstly, its moment of inertia, which is proportional to the quadrupole deformation parameter β_2 [25], is large and similar to those in the SD bands in ^{36}Ar and ^{40}Ca. The strongly deformed character of this band is further supported by the observation of its preferential feeding from the low-energy component of the highly split giant dipole resonance decay of ^{46}Ti [26]. On the other hand, the lifetimes of the states in the sideband [27,28] indicate that their deformation is smaller than that of the SD band in ^{40}Ca; it should be noted, however, that these lifetimes are subject to significant uncertainties.

Since the band head of the sideband in ^{42}Ca lies at an excitation energy of 1837 keV, considerably lower than its counterparts in the neighboring Ca and Ar isotopes, it is possible to populate this structure by Coulomb excitation in order to obtain a complete set of electromagnetic matrix elements between the observed states. This includes spectroscopic quadrupole moments that are directly related to the charge distribution in a given state, as well as transitional quadrupole matrix elements, which can be used to infer the mixing between the observed structures using comparisons with state-of-the-art model calculations.

In this Letter, we report on the results of a dedicated Coulomb excitation experiment to study properties of the superdeformed band in ^{42}Ca, performed at the Laboratori Nazionali di Legnaro, Italy [29,30]. A ^{42}Ca beam of 170 MeV energy bombarded 1 mg/cm^2 thick targets of ^{208}Pb and ^{197}Au. The γ rays from Coulomb excited nuclei were measured with the three triple clusters of AGATA [31] in coincidence with backscattered projectiles, detected in the DANTE array [32,33] consisting of three microchannel plate (MCP) detectors, covering θ_{LAB} angles from 100° to 144°.

Thanks to the combination of two position-sensitive detector arrays, DANTE for charged particles and the AGATA tracking spectrometer for γ rays, the observation and Doppler correction of the γ transitions deexciting the ground state and the sideband in ^{42}Ca were possible (see Fig. 1). The γ-ray spectrum obtained with the ^{208}Pb target, Doppler corrected for the ^{42}Ca velocity, in coincidence with backscattered particles registered in one of the MCP detectors, is shown in Fig. 2. In addition to transitions resulting from Coulomb excitation of ^{42}Ca and ^{208}Pb, weaker lines at 376, 1674, and 2048 keV are observed, originating from the subbarrier transfer reaction ^{208}Pb(^{42}Ca, ^{43}Ca)^{207}Pb (as discussed in Ref. [30]).

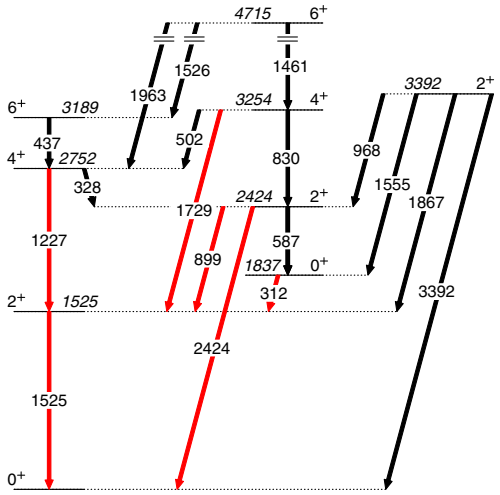

FIG. 1. Low-lying excited states in ^{42}Ca, considered in the present analysis [34]. Transitions observed in the current experiment are marked in red. Level and transition energies are given in keV.

A Doppler-broadened and shifted 511-keV γ-ray line, and transitions from Coulomb excitation of target impurities, ^{204}Pb (899 keV), ^{206}Pb (803 keV), ^{207}Pb (570 keV), are also present in the spectrum. The transition in ^{204}Pb obscured the $2_2^+ \rightarrow 2_1^+$ line in ^{42}Ca; therefore, the intensity of the latter could only be extracted from the data collected with the ^{197}Au target (see inset of Fig. 2).

A set of reduced electromagnetic matrix elements between the low-lying states in ^{42}Ca was extracted using the GOSIA code [35]. It was fitted to the observed γ-ray

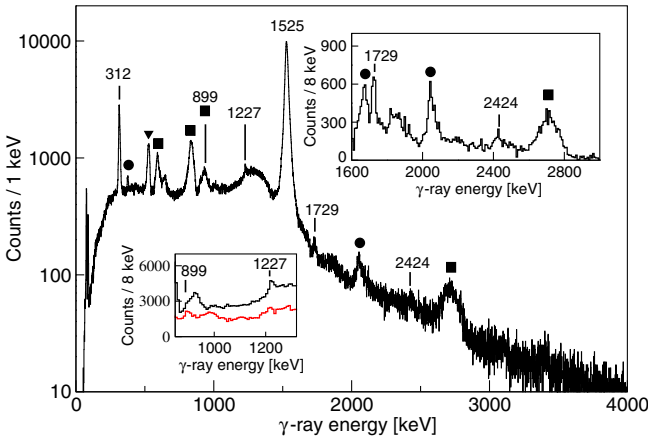

FIG. 2. The γ-ray spectrum observed in the $^{42}\mathrm{Ca} + {}^{208}\mathrm{Pb}$ Coulomb excitation experiment in coincidence with backscattered particles registered in one of the MCP detectors and Doppler corrected for the projectile. The lines not originating from ^{42}Ca are marked as follows: (filled square) lead isotopes, (filled triangle) 511 keV, (filled circle) ^{43}Ca. Insets show portions of the spectrum zoomed on the 1600–3000 keV and 850–1300 keV energy ranges, the latter also presenting the spectrum collected with the ^{197}Au target (in red, multiplied by a factor of 3 for presentation purpose).

yields, as well as to the known spectroscopic data for ^{42}Ca: lifetimes of the yrast and nonyrast states [27,36–45], $E2/M1$ mixing ratios [28,46], the quadrupole moment of the 2_1^+ state [36], and the branching ratios [45,47–49]. In particular, the $2_2^+ \rightarrow 0_1^+/2_2^+ \rightarrow 2_1^+$ branching ratio was remeasured at the Heavy Ion Laboratory, University of Warsaw, Poland, using the $^{12}\mathrm{C}(^{32}\mathrm{S}, 2p)^{42}\mathrm{Ca}$ fusion-evaporation reaction, employing the EAGLE Compton-suppressed HPGe detector array [50]. The obtained value, 0.35(7), which is in agreement with the previous findings [45], was used to constrain the Coulomb excitation data analysis. Although no transitions deexciting the 2_3^+ state were observed in the present experiment, its influence on the population of other states was taken into account by introducing into the calculations matrix elements coupling it to the observed states. These were calculated from the known spectroscopic data, such as the lifetime of the 2_3^+ state and branching and mixing ratios for all possible paths of its decay [34], and remained fixed in the GOSIA minimization routine.

It should also be noted that although the $2_2^+ \rightarrow 0_2^+$ transition is too weak to be observed, the corresponding matrix element affects excitation cross sections of observed states, in particular, that of the 2_2^+, and hence it could be determined from the intensities measured in the present Coulomb excitation experiment.

The resulting set of reduced matrix elements in ^{42}Ca and corresponding $B(E2)$ values are presented in Table I. Two key pieces of information regarding the deformation of the sideband have been obtained for the first time: the $\langle 2_2^+ \| E2 \| 0_2^+ \rangle$ matrix element, as well as the spectroscopic quadrupole moment of the 2_2^+ state. Their values are consistent with a large quadrupole deformation of this band. Other matrix elements obtained in the present analysis are in general agreement with the results of earlier measurements, and in several cases the precision has been considerably improved, notably for transitions deexciting the 4_2^+ state.

In order to get a complete picture of the coexisting structures in ^{42}Ca, two new SM and BMF calculations have been performed.

Following the previous description [13] of the spherical, normal-deformed and superdeformed structures in ^{40}Ca, SM calculations have been carried out using up to 6 particle-hole excitations from the $s_{1/2}$ and $d_{3/2}$ orbitals into the pf orbitals. This is computationally challenging, with matrices of dimensions $O(10^9)$, and was tackled using the m-scheme code ANTOINE [51,52]. The effective charges used were $1.5e$ for protons and $0.5e$ for neutrons. The results show that the configuration of the 0_2^+ and 2_2^+ states is dominated by the $6p$-$4h$ excitation, which is supported by the α transfer strength to the 0_2^+ state in ^{42}Ca measured with the $^{38}\mathrm{Ar}(^6\mathrm{Li}, d)^{42}\mathrm{Ca}$ reaction [53]. The above results are in agreement with the earlier deformed-basis antisymmetrized molecular dynamics calculations with the generator coordinate method (AMD + GCM) [54] that predicted $\beta = 0.43$ for the band built on the 0_2^+ state of the $6p$-$4h$

TABLE I. Reduced transitional and diagonal $E2$ matrix elements between the low-lying states in ^{42}Ca and corresponding $B(E2)$ values and spectroscopic quadrupole moments. Present experimental results are compared with previously measured values, SM and BMF calculations.

	$\langle I_i \| E2 \| I_f \rangle$ [e fm^2]			$B(E2\downarrow; I_i^+ \to I_f^+)$ [W.u.]	
$I_i^+ \to I_f^+$	Present	SM	BMF	Present	Previous
$2_1^+ \to 0_1^+$	$20.5^{+0.6}_{-0.6}$	11.5	9.14	$9.7^{+0.6}_{-0.6}$	9.3 ± 1 [36] 11 ± 2 [28] 9 ± 3 [27] 8.5 ± 1.9 [45]
$4_1^+ \to 2_1^+$	$24.3^{+1.2}_{-1.2}$	11.3	12.2	$7.6^{+0.7}_{-0.7}$	50 ± 15 [28] 11 ± 3 [27] 10^{+10}_{-8} [45]
$6_1^+ \to 4_1^+$	$9.3^{+0.2}_{-0.2}$	8.2	14.3	$0.77^{+0.03}_{-0.03}$	0.7 ± 0.3 [27]
$0_2^+ \to 2_1^+$	$22.2^{+1.1}_{-1.1}$	11.9	6.1	57^{+6}_{-6}	64 ± 4 [27] 100 ± 6 [28] 55 ± 1 [42] 64 ± 4 [45]
$2_2^+ \to 0_1^+$	$-6.4^{+0.3}_{-0.3}$	9.4	4.4	$1.0^{+0.1}_{-0.1}$	2.2 ± 0.6 [28] 1.5 ± 0.5 [27] 1.2 ± 0.3 [45]
$2_2^+ \to 2_1^+$	$-23.7^{+2.3}_{-2.7}$	−13.6	−7.7	$12.9^{+2.5}_{-2.5}$	17 ± 11 [28] 19^{+22}_{-14} [27] 14^{+35}_{-9} [45]
$4_2^+ \to 2_1^+$	42^{+3}_{-4}	21.9	10.1	23^{+3}_{-4}	30 ± 11 [28] 16 ± 5 [27] 12^{+7}_{-4} [45]
$2_2^+ \to 0_2^+$	26^{+5}_{-3}	32	42	15^{+6}_{-4}	< 61 [27] < 46 [45]
$4_2^+ \to 2_2^+$	46^{+3}_{-6}	52	70	27^{+4}_{-6}	60 ± 30 [27] 60 ± 20 [28] 40^{+40}_{-30} [45]
	$\langle I_i \| E2 \| I_f \rangle$ [e fm^2]			Q_{sp} [e fm^2]	
$2_1^+ \to 2_1^+$	-16^{+9}_{-3}	−4.3	0.1	-12^{+7}_{-2}	-19 ± 8 [36]
$2_2^+ \to 2_2^+$	-55^{+15}_{-15}	−31	−42	-42^{+12}_{-12}	

configuration. Furthermore, the importance of triaxiality in this system has been clearly revealed: the spectroscopic quadrupole moment of the 2_3^+ state has been found to be of similar magnitude (19 e fm^2) but of opposite sign to that of the 2_2^+ state. In addition, the calculations yielded a low-lying 3^+ state, which is connected by a strong transition to the 2_3^+ state [$B(E2; 3^+ \to 2_3^+) = 372\ e^2$ fm^4] and has a spectroscopic quadrupole moment close to zero. Hence, these states were identified as members of the SD γ band built on the 2_3^+ level, having a structure dominated by the $6p$-$4h$, similar to that of the 2_2^+ and 0_2^+ states. Constrained Hartree-Fock calculations (CHFSM) performed with the same Hamiltonian and within the same valence space [55] presented in Fig. 3(a)revealed a first triaxial minimum at $\beta = 0.4$ and with γ close to 20°, and a second minimum at $\beta = 0.6$ and $\gamma = 8°$. In contrast, the ground-state band is based on a spherical minimum, dominated by a two-particle

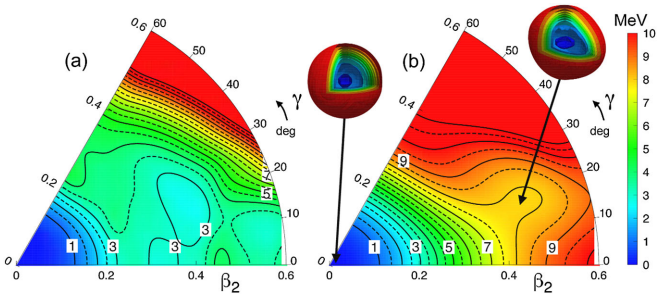

FIG. 3. Potential energy surfaces resulting from deformation-constrained Hartree-Fock calculations with (a) SM interaction, and, (b) BMF, variation after the particle number projection (PNVAP), Gogny D1S interaction. Spatial densities corresponding to each minimum found in BMF calculations are also shown in (b).

configuration, but with a considerable amount of $4p$-$2h$ and $6p$-$4h$ admixtures.

In the BMF calculations, particle number and angular momentum symmetry restorations have been taken into account as well as quadrupole (axial and nonaxial) shape mixing within a generator coordinate method. The Gogny D1S interaction was used to define the corresponding energy density functional [56]. These calculations yielded a similar general picture of a spherical ground-state band, a deformed triaxial rotational band built on top of the 0_2^+ state, and a γ band associated to it.

Matrix elements calculated using these two approaches are presented in Table I. The general picture of two coexisting structures differing in collectivity is well reproduced. However, both theoretical predictions overestimate in-band matrix elements in the sideband, and underestimate the corresponding spectroscopic quadrupole moments, which suggests that this structure may be more axially symmetric and slightly less deformed than that predicted by theory. On the other hand, quadrupole moments and transition probabilities in the ground-state band are underestimated by both models, as well as intraband transition rates, which means that the mixing between the two bands is not fully reproduced.

Comparisons of individual matrix elements may not always be conclusive; thus, the obtained $E2$ matrix elements, both experimental and theoretical, were further interpreted in the framework of the quadrupole sum method [57–59] in order to extract information on the charge distribution of the nucleus in specific states. In this method, which has been recently applied to $^{182-188}$Hg [60] and ^{96,98}Sr [61], the quadrupole rotational invariants, $\langle Q^2 \rangle$ and $\langle Q^3 \cos(3\delta) \rangle$, are calculated from experimentally determined matrix elements. The first of them is a measure of overall deformation and is proportional to the sum of squared $E2$ matrix elements $\langle i \| E2 \| t \rangle \langle t \| E2 \| i \rangle$ over all intermediate states $|t\rangle$ that can be reached from the state in question $|i\rangle$ in a single $E2$ transition. The higher-order invariant $\langle Q^3 \cos(3\delta) \rangle$ that provides information on axial symmetry is constructed of triple products of $E2$ matrix

TABLE II. Experimental and theoretical shape parameters $\langle Q^2 \rangle$ [e^2 fm^4], $\sigma(Q^2)$ [e^2 fm^4], and $\langle \cos(3\delta) \rangle$, calculated from $\langle Q^3 \cos(3\delta) \rangle$ as in Ref. [60,62].

State	$\langle Q^2 \rangle_{\rm exp}$	$\langle Q^2 \rangle_{\rm SM}$	$\sigma(Q^2)_{\rm SM}$	$\langle Q^2 \rangle_{\rm BMF}$	$\sigma(Q^2)_{\rm BMF}$
0_1^+	500 (20)	240	470	100	250
2_1^+	900 (100)	250	490	100	310
0_2^+	1300 (230)	1200	500	1900	520
2_2^+	1400 (250)	1130	500	1900	300
State	$\langle \cos(3\delta) \rangle_{\rm exp}$	$\langle \cos(3\delta) \rangle_{\rm SM}$		$\langle \cos(3\delta) \rangle_{\rm BMF}$	
0_1^+	0.06 (10)	0.34		0.34	
0_2^+	0.79 (13)	0.67		0.49	

elements ($\langle i \| E2 \| t \rangle \langle t \| E2 \| u \rangle \langle u \| E2 \| i \rangle$, where $|i\rangle$ is initial state, $|t\rangle$ and $|u\rangle$ are intermediate states), and thus relative signs of $E2$ matrix elements entering the sum must be known.

The $\langle Q^2 \rangle$ parameters were obtained for the 0^+ and 2^+ states in both bands, as presented in Table II. Since the present measurement yielded relative signs of $E2$ matrix elements coupling the 0^+ and 2^+ states, it was also possible to determine the $\langle Q^3 \cos(3\delta) \rangle$ invariants for the 0_1^+ and 0_2^+ states (Table II). This is the first time that this kind of information has been obtained in the $A \sim 40$ mass region.

The same procedure was applied to matrix elements resulting from theoretical calculations. In this case one can include in the calculations all intermediate states obtained from the theory, or just the same subset of states that were used to calculate experimental values of $\langle Q^2 \rangle$ and $\langle Q^3 \cos(3\delta) \rangle$. The difference between the results of these two approaches is negligible for all studied states in ^{42}Ca.

A simplistic interpretation of the obtained shape parameters would be that a highly deformed, nonaxial sideband coexists with the ground-state band, that is less deformed and maximally triaxial. However, ^{42}Ca, lying only 2 neutrons above the closed $N = 20$ shell, is widely considered to be spherical in its ground state, as supported by the potential energy surface maps in Fig. 3. The nonzero $\langle Q^2 \rangle$ value obtained for the 0_1^+ state may thus correspond to fluctuations about a spherical shape. This is consistent with the maximum triaxiality obtained for this state, which in this case would result from averaging over all possible quadrupole shapes. If this interpretation is correct, the dispersion of $\langle Q^2 \rangle$, defined as $\sigma(Q^2) = \sqrt{\langle Q^4 \rangle - \langle Q^2 \rangle^2}$ [63], should be comparable to $\langle Q^2 \rangle$. The existing set of experimentally determined matrix elements, although large, is not sufficient to obtain the $\langle Q^4 \rangle$ invariant. However, it can be determined from the theoretical values of matrix elements in order to get a better understanding of the experimental results.

The behavior of $\langle Q^2 \rangle$ and its dispersion is remarkably consistent for both theoretical approaches, as shown in Table II. For the ground-state band, $\sigma(Q^2)_{\rm SM}$ and $\sigma(Q^2)_{\rm BMF}$ values are comparable with $\langle Q^2 \rangle$, as one would expect for fluctuations in a spherical minimum of potential. For the sideband, however, the dispersion is much lower than the actual value, which is interpreted as a static deformation. In this case, the $\langle Q^2 \rangle$ and $\langle Q^3 \cos(3\delta) \rangle$ invariants can be further converted to the β and γ collective model deformation parameters, as explained in detail in Ref. [59].

The $\beta = 0.43(2)$ and $\gamma = 13(^{+5}_{-6})^\circ$ deformation parameters obtained in this way for 0_2^+ show that the sideband in ^{42}Ca has a slightly triaxial superdeformed shape, and can be directly compared to model predictions. A very good overall agreement is found: both potential energy surface maps presented in Fig. 3, in addition to a spherical minimum for the ground-state band, show a triaxial minimum that is located at $\beta_2 = 0.4$ and $\gamma \approx 20^\circ$ for CHFSM [Fig. 3(a)] and at $\beta_2 = 0.5$, $\gamma = 15^\circ$ for BMF calculations [Fig. 3(b)].

It should be noted that the deformation predicted by both theoretical approaches remains constant within each band. This is confirmed by the experimental results for the highly deformed structure, but those for the ground-state band show that the $\langle Q^2 \rangle$ for the 2_1^+ state is considerably larger than the value obtained for the ground state. This effect can be attributed to a possible mixing of the 2^+ states, consistent with one-neutron transfer reaction spectroscopy [64,65] and the measured intraband transition strengths that are underestimated by both calculations.

In conclusion, the properties of low-lying states in ^{42}Ca were studied via the measurement of $E2$ matrix elements using low-energy Coulomb excitation. The quadrupole deformation parameters of the ground state and the sidebands in ^{42}Ca were determined from the measured reduced matrix elements and compared with the results of SM and BMF calculations. The nonzero value of the overall deformation parameter $\langle Q^2 \rangle$ for the ground state in ^{42}Ca has been attributed to the fluctuations around the spherical shape. In contrast, a large static deformation of $\beta = 0.43(2)$ and $\beta = 0.45(2)$, respectively, was observed for the two lowest states in the sideband, proving its superdeformed character; therefore, for the first time, the deformation of a SD band was studied using the Coulomb excitation technique. The triaxiality parameter $\langle \cos(3\delta) \rangle$ measured for the 0_2^+ state provides the first experimental evidence for nonaxial character of SD bands in the $A \sim 40$ mass region. Both SM and BMF calculations well reproduce the general picture of coexistence of a spherical ground-state band with a slightly triaxial SD band. The correct description of the observed mixing between the two coexisting structures remains a challenge for future theoretical works.

The authors would like to thank Jacek Dobaczewski for fruitful discussions. We also would like to thank the members of AGATA and EAGLE Collaborations for their hard work for the project. Special gratitude goes to the INFN LNL and HIL Warsaw technical staff for their support and help, in particular, the accelerator crews for

providing intense and good-quality ^{42}Ca and ^{32}S beams. K. H.-K. acknowledges support from the Research Council of Norway under the project Grant No. 213442. T. R. R. acknowledges computing time at GSI-Darmstadt and support from Spanish MINECO under Programa Ramon y Cajal 11420 and FIS-2014-53434-P, H. N. acknowledges support from Helmholtz Association through the Nuclear Astrophysics Virtual Institute NAVI (No. VH-VI-417). We also acknowledge the support by Generalitat Valenciana, Spain, under the grant PROMETEOII/2014/019 and by the FEDER funds of the European Commission (A. Gadea), Spanish Ministerio de Economía y Competitividad under Contract No. FPA2014-57196-C5 (A. J., A. Gadea), German Bundesministerium für Bildung und Forschung (BMBF) under Contract No. 05P12PKFNE TP4 (B. Birkenbach), the Polish National Science Centre under Projects No. DEC-2013/10/M/ST2/00427, No. DPN/N190/AGATA/2009, No. 2011/03/B/ST2/01894, No. UMO-2014/14/M/ST2/00738 (COPIN-INFN Collaboration), and No. 2015/17/B/ST2/01534.

[1] S. M. Polikhanov, V. A. Druin, V. A. Karnaukov, V. L. Mikheev, A. A. Pleve, N. K. Skobelev, V. G. Subbotin, G. M. Ter-Akopyan, and V. A. Fomichev, Sov. Phys. JETP **15**, 1016 (1962).
[2] P. J. Twin *et al.*, Phys. Rev. Lett. **57**, 811 (1986).
[3] P. J. Nolan, A. Kirwan, D. J. G. Love, A. H. Nelson, D. J. Unwin, and P. J. Twin, J. Phys. G **11**, L17 (1985).
[4] E. M. Beck, F. S. Stephens, J. C. Bacelar, M. A. Deleplanque, R. M. Diamond, J. E. Draper, C. Duyar, and R. J. McDonald, Phys. Rev. Lett. **58**, 2182 (1987).
[5] E. F. Moore *et al.*, Phys. Rev. Lett. **63**, 360 (1989).
[6] E. Ideguchi *et al.*, Phys. Rev. Lett. **87**, 222501 (2001).
[7] C. E. Svensson *et al.*, Phys. Rev. Lett. **85**, 2693 (2000).
[8] C. E. Svensson *et al.*, Phys. Rev. C **63**, 061301(R) (2001).
[9] D. Rudolph *et al.*, Phys. Rev. C **65**, 034305 (2002).
[10] E. Ideguchi *et al.*, Phys. Lett. B **686**, 18 (2010).
[11] D. C. O'Leary, M. A. Bentley, B. A. Brown, D. E. Appelbe, R. A. Bark, D. M. Cullen, S. Ertürk, A. Maj, and A. C. Merchant, Phys. Rev. C **61**, 064314 (2000).
[12] E. Caurier, F. Nowacki, and A. Poves, Phys. Rev. Lett. **95**, 042502 (2005).
[13] E. Caurier, J. Menendez, F. Nowacki, and A. Poves, Phys. Rev. C **75**, 054317 (2007).
[14] T. Inakura, S. Mizutori, M. Yamagami, and K. Matsuyanagi, Nucl. Phys. **A710**, 261 (2002).
[15] R. R. Rodriguez-Guzman, J. L. Egido, and L. M. Robledo, Int. J. Mod. Phys. E **13**, 139 (2004).
[16] M. Bender, H. Flocard, and P. H. Heenen, Phys. Rev. C **68**, 044321 (2003).
[17] M. Kimura and H. Horiuchi, Nucl. Phys. **A767**, 58 (2006).
[18] Y. Taniguchi, M. Kimura, Y. Kanada-En'yo, and H. Horiuchi, Phys. Rev. C **76**, 044317 (2007).
[19] M. Kimura and H. Horiuchi, Phys. Rev. C **69**, 051304 (2004).
[20] Y. Kanada-En'yo and M. Kimura, Phys. Rev. C **72**, 064322 (2005).
[21] Y. Taniguchi, Y. Kanada-En'yo, and M. Kimura, Prog. Theor. Phys. **121**, 533 (2009).
[22] Y. Taniguchi, Y. Kanada-En'yo, and M. Kimura, Phys. Rev. C **80**, 044316 (2009).
[23] W. J. Gerace and A. M. Green, Nucl. Phys. **123**, 241 (1969).
[24] W. J. Gerace and J. P. Mestre, Nucl. Phys. **285**, 253 (1977).
[25] M. Lach *et al.*, Eur. Phys. J. A **16**, 309 (2003).
[26] M. Kmiecik *et al.*, Acta Phys. Pol. **B36**, 1169 (2005).
[27] R. Hartmann and H. Grawe, Nucl. Phys. **164**, 209 (1971).
[28] N. Lawley, N. Dawson, G. D. Jones, I. G. Main, P. J. Mulhern, R. D. Symes, and M. F. Thomas, Nucl. Phys. **159**, 385 (1970).
[29] K. Hadyńska-Klęk *et al.*, Acta Phys. Pol. B **42**, 817 (2011).
[30] K. Hadyńska-Klęk *et al.*, Acta Phys. Pol. B **44**, 617 (2013).
[31] S. Akkoyun *et al.*, Nucl. Instrum. Methods Phys. Res., Sect. A **668**, 26 (2012).
[32] A. Gadea *et al.*, Nucl. Instrum. Methods A **654**, 88 (2011).
[33] J. J. Valiente-Dobón *et al.*, Acta Phys. Pol. **B37**, 225 (2006).
[34] Balraj Singh and John A. Cameron, Nucl. Data Sheets **92**, 1 (2001).
[35] T. Czosnyka, D. Cline, and C. Y. Wu, Am. Phys. Soc. **28**, 745 (1982); www.slcj.uw.edu.pl/gosia.
[36] C. W. Towsley, D. Cline, and R. N. Horoshko, Nucl. Phys. **A204**, 574 (1973).
[37] A. R. Poletti, B. A. Brown, D. B. Fossan, P. Gorodetzky, J. J. Kolata, J. W. Olness, and E. K. Warburton, Phys. Rev. C **10**, 997 (1974).
[38] K. P. Lieb and M. Uhrmacher, Z. Phys. **267**, 399 (1974).
[39] M. Marmor, S. Cochavi, and D. B. Fossan, Phys. Rev. Lett. **25**, 1033 (1970).
[40] T. Nomura, C. Gil, H. Saito, T. Yamazaki, and M. Ishihara, Phys. Rev. Lett. **25**, 1342 (1970).
[41] R. A. Mendelson and R. T. Carpenter, Phys. Rev. **181**, 1552 (1969).
[42] P. M. Lewis, A. R. Poletti, M. J. Savage, and C. L. Woods, Nucl. Phys. **A443**, 210 (1985).
[43] R. Hartmann, K. P. Lieb, and H. Röpke, Nucl. Phys. **123**, 437 (1969).
[44] P. Betz, E. Bitterwolf, B. Busshardt, and H. Röpke, Z. Phys. A **276**, 295 (1976).
[45] W. J. Kossler, J. Winkler, and C. D. Kavaloski, Phys. Rev. **177**, 1725 (1969).
[46] H. L. Scott, R. N. Horoshko, and D. M. Van Patter, Nucl. Instrum. Methods **70**, 320 (1969).
[47] P. M. Endt and C. van der Leun, Nucl. Phys. **214**, 1 (1973).
[48] K. Kawade, H. Yamamoto, K. Yoshikawa, K. Iizawa, I. Kitamura, S. Amemiya, T. Katoh, and Y. Yoshizawa, J. Phys. Soc. Jpn. **29**, 43 (1970).
[49] P. C. Rogers and G. E. Gordon, Phys. Rev. **129**, 2653 (1963).
[50] J. Mierzejewski *et al.*, Nucl. Instrum. Methods A **659**, 84 (2011).
[51] A. Caurier and F. Nowacki (unpublished), http://www.iphc.cnrs.fr/nutheo/code_antoine/menu.html.
[52] E. Caurier, G. Martinez-Pinedo, F. Nowacki, A. Poves, and A. P. Zuker, Rev. Mod. Phys. **77**, 427 (2005).
[53] H. T. Fortune, R. R. Betts, J. N. Bishop, M. N. I. AL-Jadir, and R. Middleton, Nucl. Phys. **294**, 208 (1978).
[54] Y. Taniguchi, Prog. Theor. Exp. Phys. (2014) 073D01.

[55] B. Bounthong, Ph.D. Thesis, Université de Strasbourg (unpublished).
[56] T. R. Rodriguez and J. L. Egido, Phys. Rev. C **81**, 064323 (2010).
[57] D. Cline, Annu. Rev. Nucl. Part. Sci. **36**, 683 (1986).
[58] K. Kumar, Phys. Rev. Lett. **28**, 249 (1972).
[59] J. Srebrny and D. Cline, Int. J. Mod. Phys. E **20**, 422 (2011).
[60] N. Bree *et al.*, Phys. Rev. Lett. **112**, 162701 (2014).
[61] E. Clément *et al.*, Phys. Rev. Lett. **116**, 022701 (2016).
[62] K. Wrzosek-Lipska *et al.*, Phys. Rev. C **86**, 064305 (2012).
[63] J. Srebrny *et al.*, Nucl. Phys. **A766**, 25 (2006).
[64] C. Ellegaard, J. R. Lien, O. Nathan, G. Sletten, F. Ingebretsen, E. Osnes, P. O. Tjøm, O. Hansen, and R. Stock, Phys. Lett. **40B**, 641 (1972).
[65] A. Jamshidi and W. P. Alford, Phys. Rev. C **8**, 1782 (1973).